infrastructures

Article

Seismic Resistant Bridge Columns with NiTi Shape Memory Alloy and Ultra-High-Performance Concrete

Hadi Aryan

Viterbi School of Engineering, University of Southern California, Los Angeles, CA 90089, USA; haryan@usc.edu

Received: 27 October 2020; Accepted: 19 November 2020; Published: 30 November 2020

Abstract: Reinforced concrete bridge columns often endure significant damages during earthquakes due to the inherent deficiencies of conventional materials. Superior properties of the new materials such as shape memory alloy (SMA) and ultra-high-performance concrete (UHPC), compared to the reinforcing steel and the normal concrete, respectively, are needed to build a new generation of seismic resistant columns. Application of SMA or UHPC in columns has been separately studied, but this paper aims to combine the superelastic behavior of NiTi SMA and the high strength of UHPC, in order to produce a column design with minimum permanent deformation and high load tolerance subjected to strong ground motions. Additionally, the excellent corrosion resistance of NiTi SMA and the dense and impermeable microstructure of UHPC ensure the long-term durability of the proposed earthquake resistant column design. The seismic performance of four columns, defined as steel reinforced concrete (S-C), SMA reinforced concrete (SMA-C), SMA reinforced UHPC (SMA-UHPC), and reduced SMA reinforced UHPC (R-SMA-UHPC) is analyzed through a loading protocol with up to 4% drift cycles. The use of NiTi SMA bars for the SMA reinforced columns is limited to the plastic hinge region where permanent deformations happen. All the columns have 2.0% reinforcement ratio, except the R-SMA-UHPC column that has a 1.33% reinforcement ratio to optimize the use of SMA bars. Unlike the S-C column that showed up to 68% residual deformation compared to peak displacement during the last loading cycle the SMA reinforced columns did not experience permanent deformation. The SMA-C and R-SMA-UHPC columns showed similar strengths to the S-C column, but with about 5.0- and 6.5-times larger ductility, respectively. The SMA-UHPC column showed 30% higher strength and 7.5 times larger ductility compared to the S-C column.

Keywords: NiTi shape memory alloy; ultra-high-performance concrete; bridge column; earthquake

1. Introduction

Besides durability issues involved with normal concrete and reinforcing steel these conventional materials provide insufficient seismic capacity for the bridge columns. Development of new materials, such as shape memory alloy (SMA) and ultra-high-performance concrete (UHPC), with excellent durability and mechanical properties provides the opportunity to improve the performance of bridge columns against strong earthquakes. Accordingly, SMA and UHPC have been evaluated and implemented through various designs for improving the seismic performance of structures [1–3].

Different types of SMA such as NiTi SMA [4], Cu-based SMA [5], and Fe-based SMA [6] have been investigated for their mechanical and durability properties. One of the unique properties of SMAs, especially NiTi and Cu-based types, is the superelastic behavior that allows the material to retain its original shape after unloading, and dissipate energy through cycles of flag-shaped hysteretic loops [7,8]. SMAs have been used through different techniques to mitigate the earthquake effects on structures. For example, SMA dampers are utilized in bridges [9] and buildings [10] to improve the damping and frequency response of these structure; SMA braces are proposed to retrofit bridges [11,12] and buildings [13] against seismic excitations; and SMA restrainers are used in bridges to control the relative movements of superstructure and the response of piers [14–17]. Moreover, base isolation systems are equipped with the SMAs to mitigate the seismic actions on bridges and buildings [5,18]. Applications of SMAs also include reinforced concrete elements [19], steel beam-column connections [20], and even marine structures [21–23].

UHPC is distinguished among cement-based materials including normal concrete due to its excellent compressive strength and dense microstructure. While normal structural concrete has a 28 days compressive strength of about 35 MPa the compressive strength of UHPC is at least 145 MPa at this age [24]. UHPC has been used in construction of several bridges worldwide such as the Mars Hill bridge in the U.S., the Cat Point Creek bridge in the U.S., the Jakway Park bridge in the U.S., the Sherbrooke overpass in Canada, the Peace bridge in South Korea, the Wild bridge in Austria, the GSE bridge in Japan, the Kampung Linsum bridge in Malaysia, the Celakovice Pedestrian bridge in Czech Republic, the Luan Bai Dried-Canal Railway bridge in China, and the Yuan Jiahe bridge in China [25]. Outstanding workability and long-term durability of UHPC also make it an ideal material for prefabrication of bridge elements and accelerated construction industry [26]. The unique compressive strength of UHPC along with its proper integrity under tensile loads prevent column failure subjected to major earthquakes with vertical acceleration component, during which significant axial load variations and large moment demands affect the column [27]. Additionally, the dense microstructure of UHPC [28] makes it impermeable to moisture and adverse chemicals, and prevents aging reactions that often affect normal concrete [29].

Several studies have implemented NiTi SMA or UHPC to advance the seismic design of columns. Varela and Saiidi [30] evaluated a plastic hinge rubber element with NiTi SMA bars in a quarter-scale column subjected to strong earthquake motions on a shake table. The use of this new concept limited the column residual deformation to less than 0.5% after experiencing up to 7.0% drifts. Billah and Alam [31] performed an analytical study to address the lack of corrosion resistance and significant permanent deformation of regular steel reinforcements in reinforced concrete columns. They presented three concrete columns in which NiTi SMA or stainless steel bars were used in the plastic hinge region. Two columns with NiTi SMA bars in the plastic hinge region had either stainless steel or fiber reinforced polymer bars above the hinge region and one column with stainless steel bars in the plastic hinge region had fiber reinforced polymer bars above the hinge region. The bars of these hybrid reinforced concrete columns were connected with couplers above the plastic hinge region. Accordingly, they ensured the entire height of columns was reinforced with corrosion resistant reinforcing materials. They analyzed the columns under seismic loading and found the residual deformation of the columns with NiTi SMA bars to be 87% less compared to the column with stainless steel bars in the plastic hinge region. Mohebbi et al. [32] presented a posttensioned precast bridge column with plastic hinge region made of UHPC material, which was connected to the foundation with a pocket connection. They used unbonded carbon fiber reinforced polymer posttensioning tendons inside the column to minimize the permanent drifts and tested this technique on shake table through the Northridge-Rinaldi earthquake record. Results showed that the posttensioning approach for the column with UHPC in the plastic hinge region was effective in eliminating permanent deformations and increasing displacement ductility to 13.8 at maximum drift ratio of 6.9%. Farzad et al. [33] proposed a retrofitting technique for reinforced concrete columns using UHPC. They built eleven quarter-scale columns and intentionally damaged them with spalling concrete to implement their strengthening technique. They sandblasted the damaged part of columns and repaired seven columns with UHPC containing 2% and 4% steel fibers, one column with normal concrete, and left the rest unrepaired to be considered as reference. According to the column tests under constant axial load and cyclic lateral load repairing the damaged columns with UHPC shell increased the strength of columns without changing their size. Moreover, different fiber contents of UHPC resulted in similar strength gain in the columns.

Unlike previous studies on the application of NiTi SMA or UHPC in bridge columns, this paper presents a column design with a combination of NiTi SMA reinforcements and UHPC at the same time to take advantage of both materials' excellent properties against earthquake. The reduced ratio of SMA reinforcement is also evaluated in the column design with UHPC and SMA. Results of the two UHPC columns, with full and reduced ratios of NiTi SMA reinforcement, are compared with two concrete columns with SMA and steel reinforcements. In this study, the NiTi type of SMA is used, since it benefits from larger and more stable flag shaped hysteretic loops of superelastic behavior compared to the other SMA types, in order to minimize residual deformation and raise energy dissipation [34]. The NiTi SMA has a high corrosion resistance as well [35].

2. Finite Element Models

Four column sections are considered in this study, as shown in Figure 1. The columns are modeled in OpenSees program [36]. All the columns are 3.6 m high and have a diameter of 0.8 m. The steel reinforced concrete (S-C), SMA reinforced concrete (SMA-C), and SMA reinforced UHPC (SMA-UHPC) column sections are reinforced with 2.0% of steel or NiTi SMA bars, but the reduced SMA reinforced UHPC (R-SMA-UHPC) section has a reinforcement ratio of 1.33% to optimize the use of SMA bars. The SMA reinforcements are only provided at the bottom quarter of the column height, as the plastic hinge region and the top three quarters of the height is reinforced with steel bars. The SMA and steel reinforcements are connected with mechanical couplers above the plastic hinge region. Geometry and material configurations of the columns are presented in Table 1.

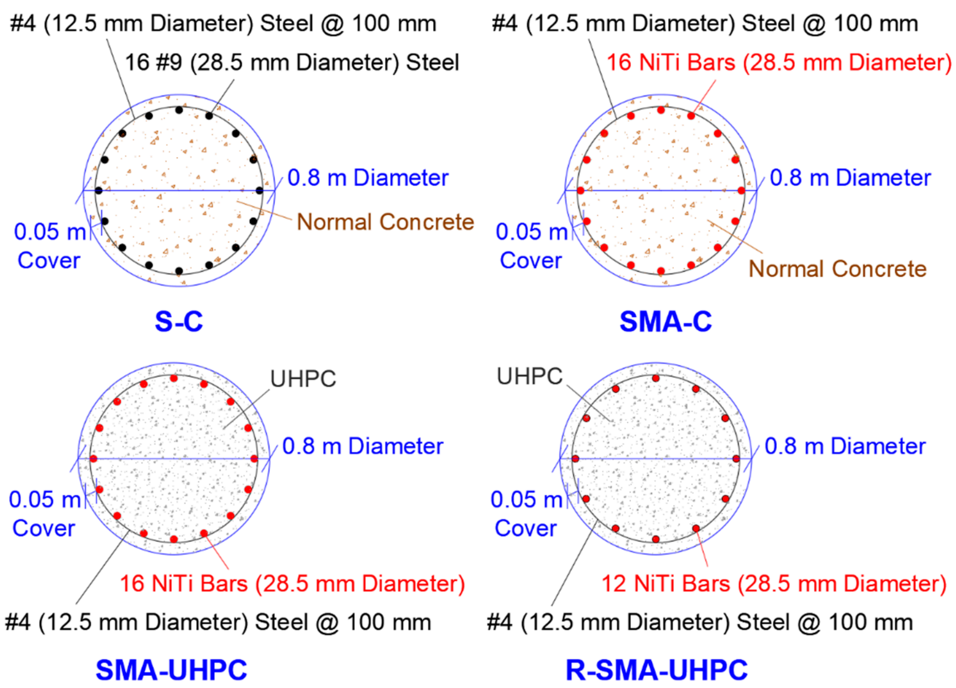

Figure 1. Column sections.

Table 1. Geometry and material configurations of columns.

Column	ID	Height (m)	Diameter (m)	Aspect Ratio	Material	Reinforcement Ratio	Section	Height Range (m)	Reinforcement Material
Steel Reinforced Concrete	S-C	3.6	0.8	4.5	Concrete	2.0%	Plastic	0–0.8	Steel
							Elastic	0.8–3.6	Steel
SMA Reinforced Concrete	SMA-C	3.6	0.8	4.5	Concrete	2.0%	Plastic	0–0.8	NiTi SMA
							Elastic	0.8–3.6	Steel
SMA Reinforced UHPC	SMA-UHPC	3.6	0.8	4.5	UHPC	2.0%	Plastic	0–0.8	NiTi SMA
							Elastic	0.8–3.6	Steel
Reduced SMA Reinforced UHPC	R-SMA-UHPC	3.6	0.8	4.5	UHPC	1.33%	Plastic	0–0.8	NiTi SMA
							Elastic	0.8–3.6	Steel

As shown in Figure 2, each column model consists of four equal-length elements along the height from which the bottom one is a distributed plasticity element, with a fiber section representing the plastic hinge region, and the top three elements are elastic. Seven equally distanced integration points are used along the distributed plasticity element with fiber section, which are not shown in Figure 2 for simplicity. According to Figure 2, the column mass is concentrated at five points along the height from which the three middle points hold the summation of mass from half of two elements below and above them, while the top and bottom points only hold the mass from half of their adjacent elements at the top and bottom, respectively. Therefore, the concentrated mass at the top and bottom points is half of the concentrated mass at the middle points.

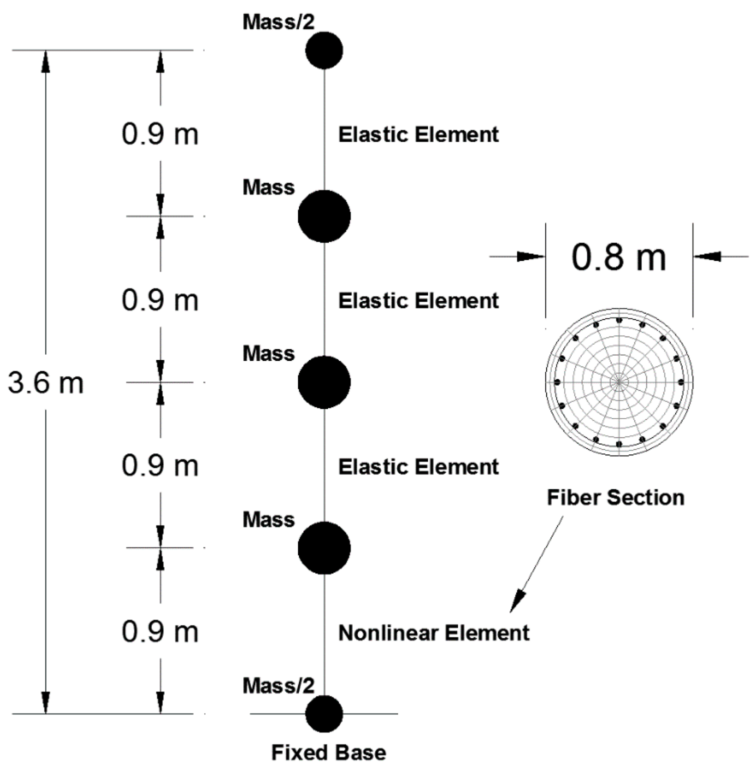

Figure 2. Column model in OpenSees.

The Concrete02, ReinforcingSteel, and SelfCentering models are used for concrete, steel, and SMA materials, respectively. The Concrete02 model properly captures the post-peak behavior of concrete during loading and unloading cycles and the ReinforcingSteel model accurately follows the linear elastic, yield plateau, and strain hardening portions of reinforcing steel behavior in concrete in opposition to the common bilinear steel models. The SelfCentering model constructs the flag-shaped and energy dissipative SMA material hysteresis behavior in uniaxial direction under tension and compression cycles [36]. The unconfined concrete has a compressive strength of 34.5 MPa, and peak and ultimate strains of 0.0022 and 0.005, respectively. The Mander model [37] is used to obtain the properties of the confined concrete. Accordingly, the confined concrete has a compressive strength of 44.1 MPa, and peak and ultimate strains of 0.0054 and 0.0128, respectively. The properties of unconfined UHPC are obtained from [24], for the case of using 6 mm straight steel fibers with 2% volumetric content in mixture. Accordingly, the unconfined UHPC has a compressive strength of 145.8 MPa, and peak and ultimate strains of 0.0044 and 0.0146, respectively. The confined UHPC has a compressive strength of 154.8 MPa, and peak and ultimate strains of 0.0137 and 0.0289, respectively. The tensile strengths of concrete and UHPC are conservatively overlooked. The stress strain behavior of confined concrete and UHPC are plotted in Figure 3. The steel reinforcement is Grade 60 with ultimate strain of 0.09, and yield and ultimate tensile strengths of 414 MPa and 621 MPa, respectively. The superelastic behavior of NiTi SMA is implemented based on [12,34], as shown in Figure 4.

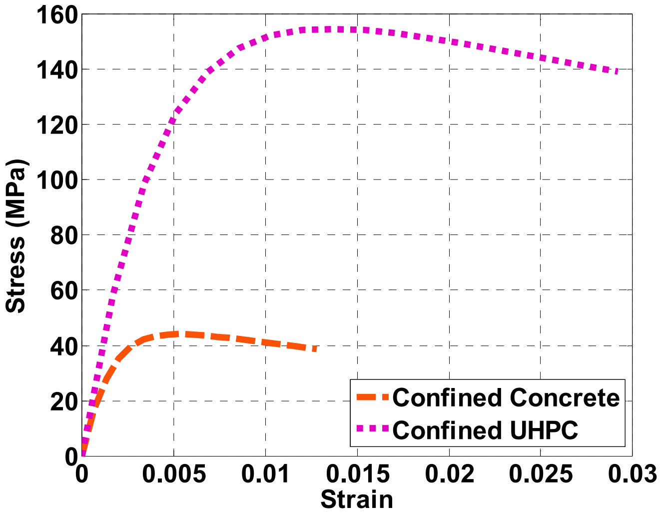

Figure 3. Stress-strain behavior of confined concrete and UHPC.

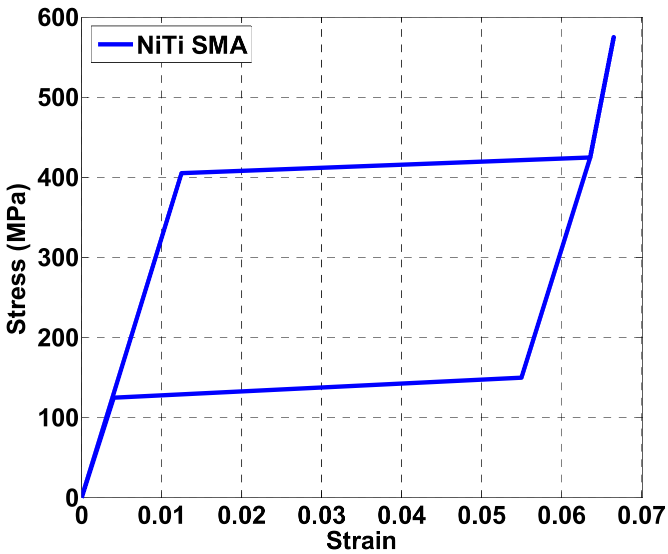

Figure 4. Superelastic behavior of NiTi SMA.

An eigenvalue analysis is performed to obtain and compare the natural periods of the columns. Then, a loading protocol consisting of a constant axial load and lateral cycles of displacement control drifts is applied to the columns as shown in Figure 5. A constant vertical load of 1735 kN is applied to the columns as the service load, which is equivalent to 10% of the compression capacity of the S-C column. The columns are also subjected to eight displacement control lateral drift cycles at the top, including two cycles of 0.5%, two cycles of 1.0%, two cycles of 2.0%, and two cycles of 4.0% drifts, while their base is assumed as fixed support. Accordingly, the capacity of columns to respond a seismic action is analyzed and compared through this loading protocol.

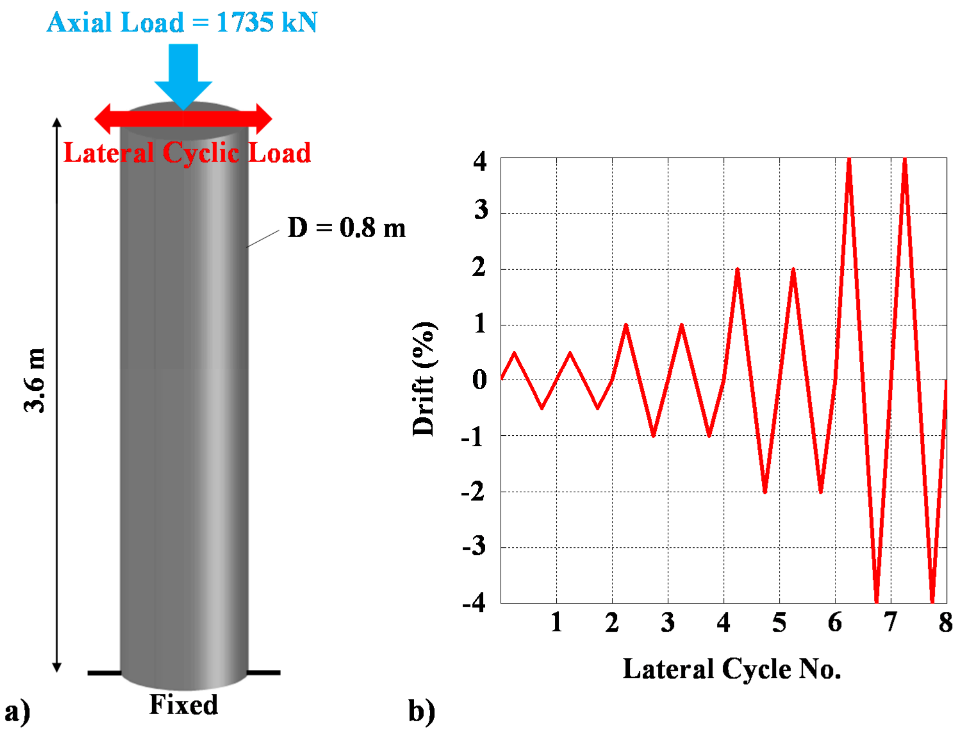

Figure 5. (**a**) Loading and boundary conditions; (**b**) lateral loading protocol.

3. Results of Analysis

According to the eigenvalue analysis the natural periods of the S-C, SMA-C, SMA-UHPC, and R-SMA-UHPC columns are 0.038, 0.040, 0.034, and 0.035 second, respectively. Based on Equation (1) and assuming mass, m, as a constant the columns with lower natural period, T, have higher initial stiffness, K. Most importantly, the columns are analyzed subjected to the lateral cyclic loading protocol and constant axial load, as explained in the previous section, to compare their seismic capacity. The base shear versus drift diagrams are shown in Figure 6 for all the columns. The essential seismic parameters to compare between different columns are the strength, residual deformation, drift ductility, and energy dissipation. The obvious difference between the behavior of the S-C column and the rest of columns with SMA reinforcement is the amount of residual deformation. During the 2.0% and 4.0% drift cycles the residual deformation of S-C column at zero load is equivalent to 0.9% and 2.7% drifts, respectively. This means that during 2.0% and 4.0% drift cycles, there is 45% and 68% residual deformation, respectively, in the S-C column, after unloading to zero load compared to the peak displacement. On the other hand, replacing the steel reinforcement with the SMA reinforcement in the plastic hinge region leads to zero residual deformation in all the SMA reinforced columns during different drift cycles. This means that the S-C column cannot be serviceable after the earthquake, but the SMA reinforced columns retain their serviceability. The S-C column shows more energy dissipation through different loading cycles compared to the other columns but, since the energy is dissipated after large permanent deformations, it would not benefit the column. In other words, the larger inside area of base shear-drift cycles diagram of the S-C column is due to the significant residual deformations and damages after returning to zero load during different drift cycles. Between the SMA reinforced columns, the SMA-C column showed slightly more energy dissipation compared to the SMA-UHPC and R-SMA-UHPC columns, especially during the initial drift cycles up to 2%.

$$T = 2\pi\sqrt{\frac{\mathrm{m}}{K}} \tag{1}$$

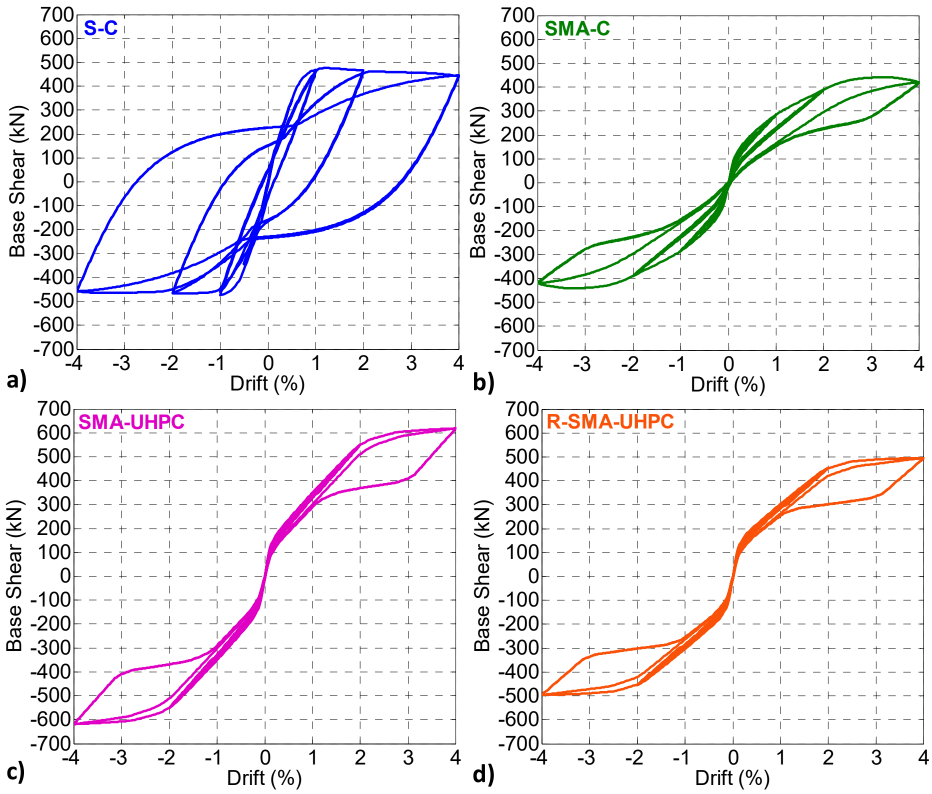

Figure 6. Base shear versus drift diagrams for different columns: (**a**) S-C, (**b**) SMA-C, (**c**) SMA-UHPC, (**d**) R-SMA-UHPC.

In order to compare the performance of different columns in terms of strength all the base shear versus drift diagrams are plotted in Figure 7 at the same time. The SMA-UHPC, R-SMA-UHPC, S-C, and SMA-C columns have shown the highest to the lowest strengths of 619 kN, 495 kN, 476 kN, and 441 kN, respectively. Therefore, the SMA-UHPC column design provides 30% higher strength compared to the S-C column, and removes the residual deformation. The R-SMA-UHPC column provides just about 4% higher strength compared to the S-C column. Accordingly, when UHPC is used along with the SMA reinforcement, reducing the reinforcement ratio by one third results in getting a similar strength to the S-C column, and still being able to remove the residual deformation. Moreover, results show that using SMA reinforcement in the plastic hinge region of the SMA-C column does not compromise the strength by more than 7% compared to the S-C column, while it prevents the permanent deformation.

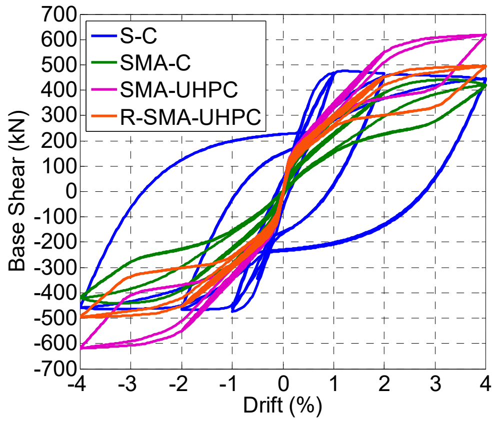

Figure 7. Base shear versus drift diagrams of the columns.

It is important to note that the UHPC columns with full and reduced ratios of SMA reinforcement reach their maximum strength at about 4.0% drift, while the concrete columns with SMA and steel reinforcements reach their peak strength at about 3.0% and 1.2% drifts, respectively. The column drift ductility, μ_D, is defined in Equation (2) as the drift at peak strength, D_{peak}, divided by the drift at yield point, D_{yeild}. Accordingly, the SMA-UHPC, R-SMA-UHPC, and SMA-C columns have a ductility of about 22, 20, and 15, respectively, while the ductility of S-C column is 3. Therefore, the SMA reinforced columns, with UHPC or concrete, provide much larger ductility than the S-C column. The R-SMA-UHPC and SMA-C columns provide similar strength to the S-C column, but their ductility is about seven and five times that of the S-C column, respectively. As summarized in Table 2, results show that the SMA-UHPC, R-SMA-UHPC, and SMA-C columns have superior seismic performance compared to the S-C column in terms of ductility and residual deformation. The SMA-UHPC column shows the best seismic performance among all the columns, given its highest strength and ductility. Due to the high corrosion resistant of NiTi SMA bars used in the plastic hinge region, and the dense and impermeable microstructure of UHPC over the entire column height, the proposed SMA-UHPC column has excellent long-term durability in addition to its extraordinary seismic performance.

$$\mu_D = \frac{D_{peak}}{D_{yeild}} \tag{2}$$

Table 2. Summary of the results.

Column	Strength (kN)	μ_D	Residual Deformation
S-C	476	3	68%
SMA-C	441	15	0%
SMA-UHPC	619	22	0%
R-SMA-UHPC	495	20	0%

As presented in Table 2, the S-C column suffered from 68% residual deformation after unloading to zero load during the last drift cycle. Figure 8 shows the distribution of corresponding residual curvature, rotation, and deflection at the plastic hinge region of S-C column in the positive and negative directions.

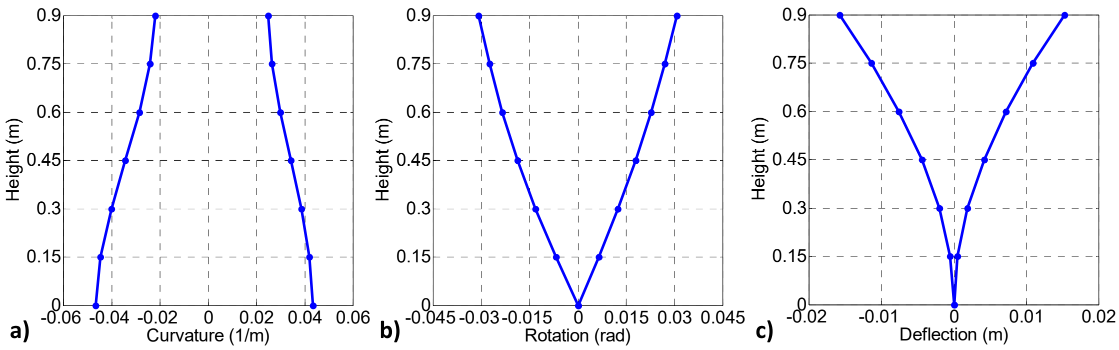

Figure 8. Residual deformation at the plastic hinge region of S-C column: (**a**) curvature, (**b**) rotation, (**c**) deflection.

Assuming linear behavior above the plastic hinge region, the residual deflection along the height of S-C column is shown in Figure 9, in comparison with its peak deflection. Elimination of this significant residual deflection as accomplished in the other columns by using the NiTi SMA bars in the plastic hinge region is crucial for immediate serviceability of the bridge after earthquake.

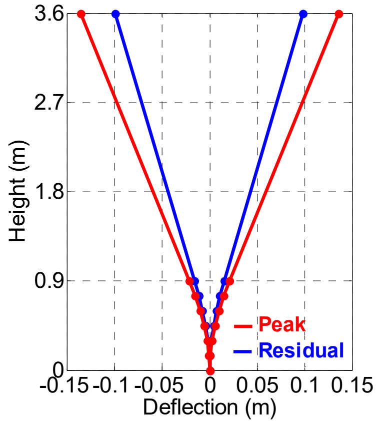

Figure 9. Residual versus peak deflections of the S-C column along the height.

4. Summary and Conclusions

NiTi SMA bars are suitable alternatives for steel reinforcement of concrete elements in seismic regions, due to their self-centering and energy dissipative properties. On the other hand, UHPC properties in terms of strength and integrity significantly outweigh the concrete properties. Among previous studies on the application of new materials in bridge columns, some have replaced the steel reinforcement with NiTi SMA bars and others utilized UHPC instead of normal concrete. Replacing steel reinforcement with NiTi SMA bars resulted in minimum permanent deformation for columns but with no strength advantage over conventional columns. On the other hand, replacing concrete with UHPC only increased the column strength, and did not reduce the residual deformations in the absence of a secondary measure. In order to take advantage of the excellent properties of both NiTi SMA and UHPC materials in the column, this study proposed and evaluated a column design made of UHPC with full and reduced ratio of NiTi SMA bars in the plastic hinge region, and compared its performance with existing designs. Four columns with 3.6 m height and 0.8 m diameter were modeled in the OpenSees finite element program. Each column model consisted of four equal-height elements from which the bottom element was nonlinearly modeled using fiber section and the top three elements were elastic. The first model was the conventional S-C column. The second model was the SMA-C column, which was similar to the first model but with NiTi SMA bars in the plastic hinge region, instead of longitudinal steel reinforcement. The third model was the SMA-UHPC column, in which the column was made of UHPC, and NiTi SMA bars were used in the plastic hinge region. The fourth model was the R-SMA-UHPC column, which was similar to the third model, but with reduced reinforcement ratio to optimize the use of SMA bars. Except for the R-SMA-UHPC column, which had 1.33% reinforcement ratio, the rest of the columns had 2.0% reinforcement. The columns were analyzed under constant axial load and lateral cyclic loading up to 4.0% drift. The main findings of the study are summarized here:

- Unlike the S-C column, which experienced 68% residual deformation the columns with NiTi SMA reinforcement did not suffer from permanent deformation.
- The strength of SMA-UHPC column, 619 kN, was about 30% higher compared to the S-C column, 476 kN.
- The strengths of SMA-C and R-SMA-UHPC columns were similar to the S-C column.
- The SMA-UHPC, R-SMA-UHPC, and SMA-C columns showed 7.5, 6.5, and 5 times larger ductility, compared to the S-C column.

Accordingly, the SMA-UHPC column showed the best seismic performance compared to the other columns in terms of strength, ductility, and residual deformation. It is also important to note that the columns made of UHPC benefit from its dense microstructure and impermeability. Moreover, the NiTi SMA bars are proven to have excellent corrosion resistance. Therefore, the SMA-UHPC and

R-SMA-UHPC designs ensure long-term durability for columns, in addition to providing excellent resilience against earthquakes.

Funding: This research received no external funding.

Conflicts of Interest: The author declares no conflict of interest.

References

1. Song, G.; Ma, N.; Li, H.-N. Applications of shape memory alloys in civil structures. *Eng. Struct.* **2006**, *28*, 1266–1274. [CrossRef]
2. Zareie, S.; Issa, A.S.; Seethaler, R.J.; Zabihollah, A. Recent advances in the applications of shape memory alloys in civil infrastructures: A review. *Structures* **2020**, *27*, 1535–1550. [CrossRef]
3. Xue, J.; Briseghella, B.; Huang, F.; Nuti, C.; Tabatabai, H.; Chen, B. Review of ultra-high performance concrete and its application in bridge engineering. *Constr. Build. Mater.* **2020**, *260*, 119844. [CrossRef]
4. Aryan, H.; Ghassemieh, M. Mitigation of Vertical and Horizontal Seismic Excitations on Bridges Utilizing Shape Memory Alloy System. *Adv. Mater. Res.* **2013**, *831*, 90–94. [CrossRef]
5. Zhang, Y.; Hu, X.; Zhu, S. Seismic performance of benchmark base-isolated bridges with superelastic Cu-Al-Be restraining damping device. *Struct. Control. Heal. Monit.* **2009**, *16*, 668–685. [CrossRef]
6. Omori, T.; Ando, K.; Okano, M.; Xu, X.; Tanaka, Y.; Ohnuma, I.; Kainuma, R.; Ishida, K. Superelastic effect in polycrystalline ferrous alloys. *Science* **2011**, *333*, 68–71. [CrossRef]
7. Desroches, R.; McCormick, J.; Delemont, M. Cyclic properties of superelastic shape memory alloy wires and bars. *J. Struct. Eng.* **2004**, *130*, 38–46. [CrossRef]
8. Rahmzadeh, A.; Alam, M.S. Seismic performance assessment of steel bridge piers with shape memory alloy in plastic hinge length. In Proceedings of the Eleventh U.S. National Conference on Earthquake Engineering, Los Angeles, CA, USA, 25–29 June 2018.
9. Sharabash, A.M.; Andrawes, B.O. Application of shape memory alloy dampers in the seismic control of cable-stayed bridges. *Eng. Struct.* **2009**, *31*, 607–616. [CrossRef]
10. Qian, H.; Li, H.; Song, G. Experimental investigations of building structure with a superelastic shape memory alloy friction damper subject to seismic loads. *Smart Mater. Struct.* **2016**, *25*, 125026. [CrossRef]
11. Aryan, H.; Ghassemieh, M. Seismic enhancement of multi-span continuous bridges subjected to three-directional excitations. *Smart Mater. Struct.* **2015**, *24*, 45030. [CrossRef]
12. Aryan, H.; Ghassemieh, M. A superelastic protective technique for mitigating the effects of vertical and horizontal seismic excitations on highway bridges. *J. Intell. Mater. Syst. Struct.* **2017**, *28*, 1533–1552. [CrossRef]
13. Moradi, S.; Alam, M.S.; Asgarian, B. Incremental dynamic analysis of steel frames equipped with NiTi shape memory alloy braces. *Struct. Des. Tall Spec. Build.* **2014**, *23*, 1406–1425. [CrossRef]
14. Alam, M.S.; Bhuiyan, M.A.R.; Billah, A.H.M.M. Seismic fragility assessment of SMA-bar restrained multi-span continuous highway bridge isolated by different laminated rubber bearings in medium to strong seismic risk zones. *Bull. Earthq. Eng.* **2012**, *10*, 1885–1909. [CrossRef]
15. Padgett, J.E.; Desroches, R.; Ehlinger, R. Experimental response modification of a four-span bridge retrofit with shape memory alloys. *Struct. Control Health Monit.* **2010**, *17*, 694–708. [CrossRef]
16. Li, S.; Dezfuli, F.H.; Wang, J.Q.; Alam, M.S. Seismic vulnerability and loss assessment of an isolated simply-supported highway bridge retrofitted with optimized superelastic shape memory alloy cable restrainers. *Bull. Earthq. Eng.* **2020**, *18*, 3285–3316.
17. Ghassemieh, M.; Kashan, S.M.G.; Khanmohammadi, M.; Baei, M. A Superelastic retrofitting method for mitigating the effects of seismic excitations on irregular bridges. *Civ. Eng. Infrastruct. J.* **2018**, *51*, 147–168.
18. Huang, B.; Zhang, H.; Wang, H.; Song, G. Passive base isolation with superelastic nitinol SMA helical springs. *Smart Mater. Struct.* **2014**, *23*, 065009. [CrossRef]
19. Abbass, A.; Attarnejad, R.; Ghassemieh, M. Seismic assessment of rc bridge columns retrofitted with near-surface mounted shape memory alloy technique. *Materials* **2020**, *13*, 1701. [CrossRef]
20. Chowdhury, A.; Rahmzadeh, A.; Alam, M.S. Improving the seismic performance of post-tensioned self-centering connections using SMA angles or end plates with SMA bolts. *Smart Mater. Struct.* **2019**, *28*, 075044. [CrossRef]

21. Zareie, S.; Alam, M.S.; Seethaler, R.J.; Zabihollah, A. Stability control of a novel frame integrated with an SMA-MRF control system for marine structural applications based on the frequency analysis. *Appl. Ocean Res.* **2020**, *97*, 102091.
22. Zareie, S.; Zabihollah, A. A semi-active SMA-MRF structural stability element for seismic control in marine structures. *Appl. Ocean Res.* **2020**, *100*, 102161.
23. Zareie, S.; Alam, M.S.; Seethaler, R.J.; Zabihollah, A. Effect of shape memory alloy-magnetorheological fluid-based structural control system on the marine structure using nonlinear time-history analysis. *Appl. Ocean Res.* **2019**, *91*, 101836.
24. Prabha, S.L.; Dattatreya, J.K.; Neelamegam, M. Stress strain behaviour of ultra high performance concrete under uniaxial compression. *Int. J. Civ. Eng. Technol.* **2014**, *5*, 187–194.
25. Zhou, M.; Lu, W.; Song, J.; Lee, G.C. Application of ultra-high performance concrete in bridge engineering. *Constr. Build. Mater.* **2018**, *186*, 1256–1267. [CrossRef]
26. Caluk, N.; Mantawy, I.M.; Azizinamini, A. Durable bridge columns using stay-in-place UHPC shells for accelerated bridge construction. *Infrastructures* **2019**, *4*, 25. [CrossRef]
27. Aryan, H.; Ghassemieh, M. Numerical assessment of vertical ground motion effects on highway bridges. *Can. J. Civ. Eng.* **2020**, *47*, 790–800. [CrossRef]
28. Chen, H.-J.; Yu, Y.-L.; Tang, C.-W. Mechanical properties of ultra-high performance concrete before and after exposure to high temperatures. *Materials* **2020**, *13*, 770. [CrossRef]
29. Alnaggar, M.; Cusatis, G.; Di Luzio, G. Lattice Discrete Particle Modeling (LDPM) of Alkali Silica Reaction (ASR) deterioration of concrete structures. *Cem. Concr. Compos.* **2013**, *41*, 45–59. [CrossRef]
30. Varela, S.; Saiidi, M.S. A bridge column with superelastic NiTi SMA and replaceable rubber hinge for earthquake damage mitigation. *Smart Mater. Struct.* **2016**, *25*, 075012. [CrossRef]
31. Billah, A.M.; Alam, M.S. Seismic performance of concrete columns reinforced with hybrid shape memory alloy (SMA) and fiber reinforced polymer (FRP) bars. *Constr. Build. Mater.* **2012**, *28*, 730–742. [CrossRef]
32. Mohebbi, A.; Saiidi, M.S.; Itani, A. Shake table studies and analysis of a PT-UHPC bridge column with pocket connection. *J. Struct. Eng.* **2018**, *144*, 04018021. [CrossRef]
33. Farzad, M.; Shafieifar, M.; Azizinamini, A. Retrofitting of bridge columns using UHPC. *J. Bridge Eng.* **2019**, *24*, 04019121. [CrossRef]
34. Dolce, M.; Cardone, D. Mechanical behaviour of shape memory alloys for seismic applications 2. Austenite NiTi wires subjected to tension. *Int. J. Mech. Sci.* **2001**, *43*, 2657–2677. [CrossRef]
35. van der Wijst, M.W.M. *Shape Memory Alloys Featuring Nitinol*; Veldhoven; Eindhoven University of Technology: Eindhoven, The Netherlands, 1992.
36. McKenna, F.; Fenves, G.L.; Scott, M.H. *Open System for Earthquake Engineering Simulation*; Pacific Earthquake Engineering Research Center: Richmond, CA, USA, 2000.
37. Mander, J.B.; Priestley, M.J.N.; Park, R. Theoretical stress-strain model for confined concrete. *J. Struct. Eng.* **1988**, *114*, 1804–1826. [CrossRef]

Publisher's Note: MDPI stays neutral with regard to jurisdictional claims in published maps and institutional affiliations.